Journal of Quantitative Spectroscopy & Radiative Transfer 104 (2007) 384–399

Journal of Quantitative Spectroscopy & Radiative Transfer

www.elsevier.com/locate/jqsrt

# Maximum time-resolved hemispherical reflectance of absorbing and isotropically scattering media

Kyle D. Smith, Kamal M. Katika, Laurent Pilon*

*Mechanical and Aerospace Engineering Department, Henry Samueli School of Engineering and Applied Science, University of California, Los Angeles, 420 Westwood Plaza, 37-132 Eng. IV, Los Angeles, CA 90095, USA*

Received 10 July 2006; accepted 13 September 2006

**Abstract**

This paper presents a parametric study of the time-resolved hemispherical reflectance of a plane-parallel slab of homogeneous, cold, absorbing, and isotropically scattering medium exposed to a collimated Gaussian pulse. The front surface of the slab is transparent while the back surface is assumed to be cold and black. The 1-D time-dependent radiation transfer equation is solved using the modified method of characteristics. The parameters explored include (1) the optical thickness, (2) the single scattering albedo of the medium, and (3) the incident pulse width. The study pays particular attention to the maximum transient hemispherical reflectance and identifies optically thin and thick regimes. It shows that the maximum reflectance is independent of the optical thickness in the optically thick regime. In the optically thin regime, however, the maximum hemispherical reflectance depends on all three parameters explored. The transition between the optically thick and thin regimes occurs when the optical thickness is approximately equal to the dimensionless pulse width. Finally, correlations relating the maximum of the hemispherical reflectance as a function of the optical thickness, the single scattering albedo of the materials, and the incident pulse width have been developed. These correlations could be used to retrieve radiation characteristics or serve as initial guesses for more complex inversion schemes accounting for anisotropic scattering.


*Keywords:* Transient radiative transfer; Method of characteristics; Scattering; Turbid media; Biological tissues; Inverse method

## 1. Introduction

Transient radiation transfer has found numerous applications in (1) laser-assisted micromachining, (2) remote sensing of combustion systems, and (3) of biological tissues among others [1]. The governing equation for radiation transfer in homogeneous, absorbing, emitting, and scattering media is the so-called radiative transfer equation (RTE). It expresses an energy balance in a unit solid angle $d\Omega$ about the direction $\hat{\mathbf{s}}$. For a non-emitting medium, on a gray basis, it can be written as [2]

$$\frac{1}{c}\frac{\partial I}{\partial t} + (\hat{\mathbf{s}} \cdot \nabla) I = -\kappa I - \sigma_s I + \frac{\sigma_s}{4\pi}\int_{4\pi} I(\hat{\mathbf{s}}_i)\Phi(\hat{\mathbf{s}}_i, \hat{\mathbf{s}})\, d\Omega_i, \tag{1}$$

*Corresponding author. Tel.: +1 310 206 5598; fax: +1 310 206 2302.
*E-mail address:* pilon@seas.ucla.edu (L. Pilon).

0022-4073/$ - see front matter 
doi:10.1016/j.jqsrt.2006.09.008

where $I$ is the intensity in the $\hat{\mathbf{s}}$-direction and $c$ is the speed of light in the medium. The linear absorption and scattering coefficients are denoted by $\kappa$ and $\sigma_s$, respectively. The first and second terms on the right-hand side of the equation represent attenuation of radiation by absorption and scattering, respectively. Finally, the last term on the right-hand side corresponds to the augmentation of radiation due to in-scattering. The scattering phase function $\Phi(\hat{\mathbf{s}}_i, \hat{\mathbf{s}})$ represents the probability that radiation propagating in the solid angle $d\Omega_i$ around direction $\hat{\mathbf{s}}_i$ will be scattered into the cone $d\Omega$ around the direction $\hat{\mathbf{s}}$. The transient RTE is an integro-differential equation involving seven independent variables. In addition, various other factors like geometry, temperature fields, and the radiation characteristics of the medium make the RTE difficult to solve.

Established techniques for estimating the absorption and scattering coefficients as well as the scattering phase function consist of measuring the spectral or total, directional–hemispherical or directional–directional transmittance and reflectance, with collimated or diffuse incident radiation. First, initial values for the radiation characteristics are assumed and the RTE is solved. The calculated and measured quantities are compared and a new estimate of the radiation characteristics is made. This procedure is accomplished in an iterative and time consuming manner until the set of absorption and scattering coefficients and scattering phase function minimizes the difference between the measured and the calculated properties. The major difficulty inherent to the inverse method is that there is no unique solution for the radiation characteristics. Moreover, due to the iterative nature of the method, the initial guess for radiation characteristics is of major importance if one wants a rapid convergence toward the optimum solution.

Moreover, Yamada and Kurosaki [3] retrieved the radiation characteristics of porous materials from emittance measurements. Indeed, the authors assumed an isotropic scattering phase function and used the fact that the emittance of an optically thick and isotropically scattering medium is independent of the optical thickness and depends only on the single scattering albedo. Finally, they recommended their method for highly scattering media rather than for absorbing media since the albedo is very sensitive to emittance and that the latter is larger for strongly absorbing media.

The present analysis aims at (1) gaining a physical understanding of transient radiation transfer in participating media, (2) performing a parametric study for the time-dependent hemispherical reflectance of a cold plane-parallel slab of an absorbing and isotropically scattering medium subject to a collimated Gaussian pulse, and (3) developing simple correlations for the maximum of the time-resolved hemispherical reflectance. The study pays particular attention to the maximum transient hemispherical reflectance which can easily be measured experimentally using a time-resolved attenuated total reflectance device [4]. Reflectance is preferred to transmittance as its magnitude and the associated signal-to-noise ratio are much larger, without requiring a powerful radiation source that could heat up or damage the samples. This issue is of particular concern for non-invasive in vivo sensing of biological tissues.

## 2. Current state of knowledge

Due to the challenges encountered in solving the RTE several simplifying approaches have been suggested. First, the diffusion approximation has been used extensively in biomedical applications [4]. Its major advantage resides in the fact that there exist analytical solutions for the time-resolved hemispherical reflectance for simple geometries [4]. Brewster and Yamada [5] used the Monte Carlo method to study the effects of single scattering albedo, optical thickness, anisotropic scattering, and detector field of view on time-resolved transmittance and reflectance of an optically thick slab subjected to a picosecond collimated pulse. The numerical results were in good agreement with predictions of the diffusion approximation at long times [5]. Brewster and Yamada propose to use their findings to retrieve the radiation characteristics of absorbing and scattering media from transient transmission measurements at long times. However, their study also indicates that the diffusion theory predictions can be poor at early times, including predictions of the maximum hemispherical reflectance and the time at which it occurs. Other studies have shown that the diffusion approximation fails to predict the transmittance at early times for all optical thicknesses and also at long times for optically thin slabs [6]. In addition, Guo et al. [7] showed that the diffusion approximation fails for both collimated radiation and strong anisotropically scattering media.

Moreover, analytical solutions of the transient RTE in homogeneous, isotropically scattering plane-parallel slab having a non-reflecting front surface with a blackbody back surface exposed to a collimated source have been obtained by Pomraning [8]. Also, Wu [9] used analytical solutions to obtain expressions for the hemispherical transmittance and reflectance. In addition, Wu [9] used the integral equation to compute the temporal reflectance and transmittance of 1-D absorbing and isotropically scattering slabs with various scattering albedos and optical thicknesses that compared well with results obtained using the Monte Carlo method. Tan and Hsu [10] used an integral formulation to simulate radiative transport in a 1-D plane-parallel slab of a homogeneous absorbing and isotropically scattering medium with a black back surface exposed to diffuse or collimated irradiation. The authors then extended the method to solve the same problem in 3-D geometries [11].

Numerical techniques have also been used to solve the transient RTE. First, in a series of papers, Kumar and co-workers solved the transient radiation transfer equation for different geometries, scattering characteristics, and boundary conditions using various methods, including the $P_1$ approximation [12], Monte Carlo [13–15], discrete-ordinates [6,16,17], and radiation element [18] methods and compared their results with predictions based on other methods or approximations [19] or with experimental data [17]. Moreover, Hsu [15] used the Monte Carlo method to study the effect of various parameters on the radiation transfer through a 1-D, plane-parallel, cold, absorbing, and isotropically scattering medium. The author focused on the transient local fluence within the slab by accounting for specular internal reflection at the slab surfaces. Elaloufi et al. [6] used a conventional discrete-ordinate method (DOM) to solve the transient RTE and assess the validity of the diffusion approximation for slabs with different radiation characteristics and anisotropy. Also, Ayranci et al. [20] used the method of lines solution of the DOM to predict transmittance of a cubical enclosure of purely scattering media. Recently, Chai et al. [21] used the finite volume method to simulate transient radiation transfer in a cube of absorbing and isotropically scattering medium with different boundary conditions and compared the results with published ones. On the other hand, Boulanger and Charette [22] used the DOM coupled with the piecewise parabolic advection (PPA) scheme to solve the transient multi-dimensional RTE for a collimated light pulse propagating in a semi-infinite, semi-transparent, non-homogeneous medium. Finally, Lu and Hsu [23] have developed the reverse Monte Carlo method in order to reduce the excessive computational time of the conventional Monte Carlo method and applied it to various geometries and scattering media. Similarly, Katika and Pilon [24] have developed the modified method of characteristics used in the present study. Advantages of this method versus other methods include its use for solving coupled equations using other numerical schemes, and its ability to capture the sharp discontinuities associated with the propagation of a radiation front in transient radiation transport.

Unfortunately, it was not possible to obtain analytical expressions [8,9] for the maximum reflectance and the time at which it occurs. Instead, a numerical parametric study is performed using the modified method of characteristics and discussed in the following sections.

## 3. Analysis

Let us consider transient radiation transfer in a homogeneous absorbing and isotropically scattering but non-emitting plane-parallel slab of thickness $L$ as shown in Fig. 1. The front surface of the slab ($z = 0$) is exposed to a normally collimated and monochromatic incident Gaussian pulse. The index of refraction of the slab is assumed to be identical to that of the surroundings and equal to unity. Thus, the entire incident light is transmitted through the front surface and internal reflection can be ignored. The back surface of the slab ($z = L$) is treated as black and cold. This can be implemented by coating the surface with paints or soot particles depending on the wavelength of interest. Finally, a Gaussian pulse is considered instead of other pulse shapes as it closely matches the shape produced by lasers or light emitting diodes.

### 3.1. Governing equation

To solve the 1-D radiative transfer equation for collimated irradiation, the intensity is split into two parts: (i) the radiation scattered from the collimated radiation source and (ii) the remaining collimated beam after partial extinction by absorption and scattering along its path. The contribution from emission by the medium

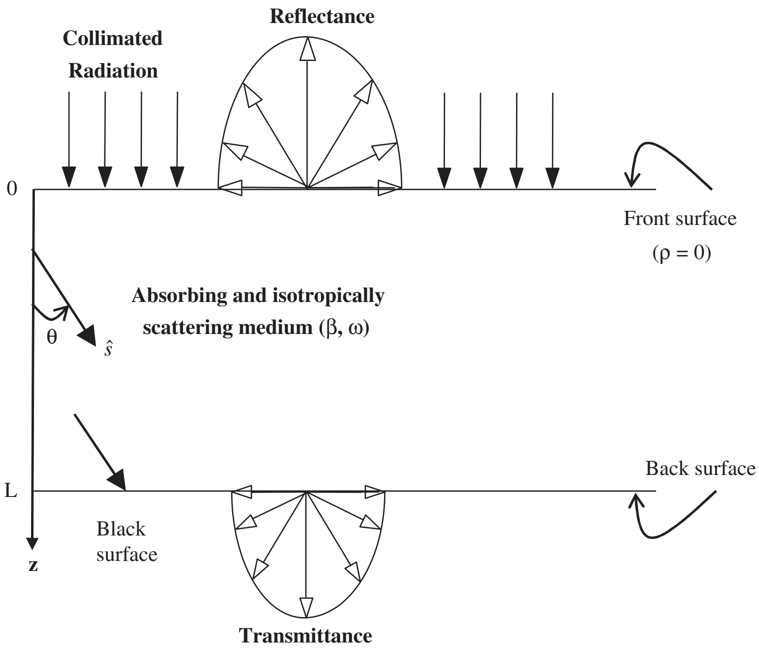


Fig. 1. Schematic of an absorbing and isotropically scattering plane-parallel slab exposed to collimated incident radiation pulse.

is negligible compared to the incident and scattered intensities, and consequently the medium can be considered as cold. Thus, the intensity for a gray medium is written as $I(z,\mu,t) = I_c(z,\mu,t) + I_d(z,\mu,t)$. The collimated intensity $I_c(z,\mu,t)$ at location $z$ and time $t$ in direction $\mu$, remnant of any incident irradiation $I_i(t)$, is given by [2,8] $I_c(z,\mu,t) = I_i(t - z/c)\delta(\mu - \mu_0)e^{-\beta z}$ where $\beta$ is the extinction coefficient ($= \kappa + \sigma_s$) and $\delta(\mu - \mu_0)$ is the Dirac's delta function. In the present case, the incident direction $\mu_0$ corresponds to the normal direction, i.e., $\mu_0 = 1$. Thus, the governing equation for the diffuse radiation intensity $I_d(z,\mu,t)$ along the characteristic curves of the photons [2,25] can be written as

$$\frac{1}{c}\frac{DI_d(z,\mu,t)}{Dt} = -\beta I_d(z,\mu,t) + \frac{\sigma_s}{4\pi}\int_{4\pi} I_d(z,\mu_i,t)\,d\Omega_i + \frac{\sigma_s}{4\pi} I_i(t - z/c)e^{-\beta z}H(t - z/c), \tag{2}$$

where $DI_d/Dt$ is the total derivative of $I_d(z,\mu,t)$ along the characteristic curves $dz/dt = c\mu$.

### 3.2. Initial and boundary conditions

In order to solve the above governing equation, initial and boundary conditions must be specified. First, the initial intensity at all locations and in all directions at time $t = 0$ is taken as zero. At subsequent times, the radiation intensity incident on the front face (at $z = 0$) is a truncated Gaussian distribution with a pulse width $t_p$ expressed as

$$I_i(t) = I_0 \exp\left[-4\ln 2\left(\frac{t - t_c}{t_p}\right)^2\right], \quad 0 < t < 2t_c \quad \text{and} \quad I_i(t) = 0, \quad t \geqslant 2t_c. \tag{3}$$

In the present study, $I_i(t)$ reaches its maximum value $I_0$ at time $t_c = 3t_p$.

Finally, for the diffuse component, $I_d$, the front is transparent while the back surface is assumed to be black and cold, i.e., $I_d(z = 0, \mu > 0, t) = 0$ and $I_d(z = L, \mu < 0, t) = 0$. The value of the diffuse intensity $I_d(z = 0, \mu < 0, t)$ and $I_d(z = L, \mu > 0, t)$ need not be considered, because the method of solution uses boundary conditions only for intensity entering the computational domain [25].

### 3.3. Dimensional analysis

Dimensional analysis of the RTE can be performed by defining the following independent dimensionless variables, $z^* = z/L$, $I^* = I/I_0$, and $t^* = t/(1/\beta c) = \beta ct$ where $L$ is the slab thickness, $I_0$ is the maximum value reached by the time-dependent incident intensity, and $1/\beta c$ represents a characteristic time for radiation propagation through the slab. Substituting the dimensionless parameters in Eq. (1) for 1-D transient radiation transfer problems along the $z$-direction yields

$$\frac{\partial I^*}{\partial t^*} + \frac{\mu}{\beta L}\frac{\partial I^*}{\partial z^*} = -I^* + \frac{\omega}{4\pi}\int_{4\pi} I^*(\hat{\mathbf{s}}_i)\Phi(\hat{\mathbf{s}}_i, \hat{\mathbf{s}})\,d\Omega_i, \tag{4}$$

where $\omega$ is the single scattering albedo defined as $\sigma_s/(\kappa + \sigma_s)$. One can also recognize the optical thickness $\beta L$. Thus, the dimensionless intensity $I^*$ at time $t^*$ and location $z^*$ in direction $\mu$ depends on the dimensionless variables $\omega$, $\beta L$, and $\Phi$, i.e., $I^* = I^*(z^*, \mu, t^*, \omega, \beta L, \Phi)$. After solving for the intensity in all directions at every time and location, the time-resolved transient hemispherical reflectance $R$ at the front surface ($z^* = 0$) can be computed based on the following definition:

$$R = -2\pi \int_{-1}^{0} I^*(0, \mu, t^*, \omega, \beta L, \Phi)\mu\,d\mu = R(t^*, \omega, \beta L, \Phi). \tag{5}$$

Furthermore, if the medium is isotropically scattering, i.e., $\Phi(\hat{\mathbf{s}}_i, \hat{\mathbf{s}}) = 1$, the transient hemispherical reflectance of the slab is a function of only three dimensionless numbers, i.e., $R = R(\beta ct, \omega, \beta L)$. Note that other characteristic times could have been selected such as: (1) the pulse width $t_p$, (2) the time at which the incident intensity reaches its maximum $t_c$, (3) the time for the pulse to travel ballistically through the slab given by $L/c$, or (4) the characteristic time of the scattering process alone defined as $t^* = \sigma_s ct$. In all cases, $\omega$, $\beta L$, and $\Phi$ appear as relevant dimensionless parameters. In addition, the dimensionless quantities $\beta ct_p$ and $\beta ct_c$ appear when time is scaled with $t_p$ and $t_c$, respectively.

### 3.4. Method of solution

The governing equation (2) and the associated boundary conditions are solved using the modified method of characteristics [25]. Extensive discussion of this method for both transient and steady-state radiation transfer has been previously reported [24,26] and need not be repeated here. Comparison between numerical integral solutions [9] and the modified method of characteristics were found to be in good agreement with a mean error of less than 5% for $\beta L = 0.5$ and $\omega = 0.05$ and 0.95 [25]. The same accuracy is expected in the present results. A uniform discretization of $N_z$ points along the $z$-direction and $N_\theta$ discrete directions for $\theta$ varying from 0 to $\pi$ was used. The time interval $\Delta t$ had little effect on the numerical results as long as it satisfied $\Delta t \leqslant \Delta z/c$. Thus, $\Delta t$ was set equal to $\Delta z/c$ where $\Delta z = L/(N_z - 1)$. After solving for the intensities in the discrete directions at every point, the hemispherical reflectance $R$ of the slab was computed from Eq. (5).

## 4. Results and discussion

A large range of optical thickness ($0 \leqslant \beta L \leqslant 50$), single scattering albedo ($0.05 \leqslant \omega \leqslant 1$), and incident pulse width ($0.015 \leqslant \beta ct_p \leqslant 0.15$) have been explored. The number of discrete points $N_z$ and directions $N_\theta$ were varied between 100 and 2000 and between 50 and 450, respectively, to obtain converged numerical solutions for each pair of parameters $\beta L$ and $\omega$. In all cases, the results were assumed to be numerically converged when doubling both $N_z$ and $N_\theta$ produced less than 1% change in the value of the computed reflectance. The integrals in Eqs. (2) and (5) were computed using the 3/8 Simpson's rule [27]. The CPU time taken for computing the transient hemispherical reflectance for the case of $\beta L = 0.5$ and $\omega = 0.95$, for example, using a spatial discretization of $N_z = 101$ points and an angular discretization of $N_\theta = 25$ directions per octant was about 21 s on a 512 MHz Pentium III for a total dimensionless time of $t^*(= \beta ct) = 8$.

### 4.1. Effect of $\beta L$ and $\omega$

Fig. 2 shows the typical transient hemispherical reflectance of the plane-parallel slab with either black or specularly reflecting back surface as a function of $\beta ct$, for $\omega = 0.7$, $\beta L = 0.5$, and $\beta ct_p = 0.15$. Since there is no direct reflection of the incident beam from the front surface, the reflected signal is due to back scattering of the incident radiation by the slab. The maximum value of the reflectance is denoted by $R_1$ and occurs at dimensionless time $\beta ct_1$. For a black back surface, the reflectance reveals only one maximum as the pulse is absorbed once it reaches the back of the slab. On the other hand, for a specularly reflecting back surface, two maxima are evident. The first one is identical to that observed with a black back surface. The second maximum corresponds to radiation emerging from the slab after being reflected by the back surface.

Moreover, Fig. 3 shows the transient hemispherical reflectance as a function of the dimensionless time $t^*$ for different values of the single scattering albedo $\omega$ and for $\beta L = 0.7$ and $\beta ct_p = 0.15$. Similar plots have been obtained for other values of $\beta L$. One can see that the hemispherical reflectance $R$ increases as $\omega$ increases for any given dimensionless time $\beta ct$. This can be attributed to the increase in the scattering coefficient resulting in a larger fraction of the incident intensity being back-scattered by the medium. It is also worth noting that the dimensionless time $\beta ct_1$ appears to be independent of $\omega$ and is equal to 0.6 in these cases.

Finally, Fig. 4 shows the transient hemispherical reflectance as a function of the dimensionless time $\beta ct$ for different values of $\beta L$ and for $\omega = 0.95$ and $\beta ct_p = 0.15$. Similar results have been obtained for different values of $\omega$. Fig. 4 indicates that the maximum reflectance $R_1$ increases with $\beta L$ up to a critical optical thickness $(\beta L)_{cr}$ beyond which it is independent of $\beta L$. The highest value for the maximum reflectance is denoted by $R_{1,max}$. One can also note that $(\beta L)_{cr}$ for this case is equal to 0.15 which, coincidentally, is also the value of $\beta ct_p$. The effect of the incident pulse width, $\beta ct_p$, will be discussed in detail in Section 4.3.

### 4.2. Maximum reflectance

Let us now focus our attention to the value of the maximum reflectance $R_1$ and its occurrence at time $\beta ct_1$ as functions of the optical thickness $\beta L$ and of the single scattering albedo $\omega$. Fig. 5 (top) shows the peak value of

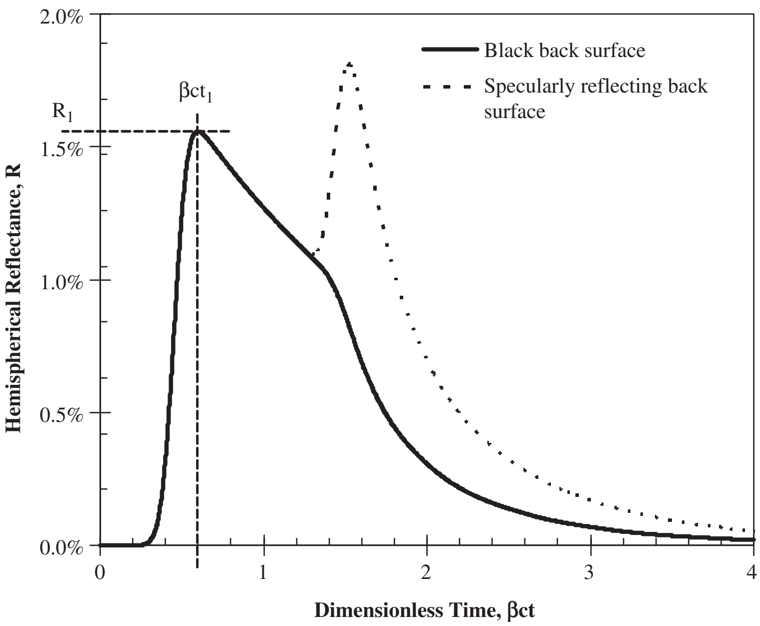


Fig. 2. Time-resolved hemispherical reflectance $R$ versus the dimensionless time $\beta ct$ for $\beta ct_p = 0.15$ with $\beta L = 0.5$ and $\omega = 0.7$ with black or specularly reflecting back surface.

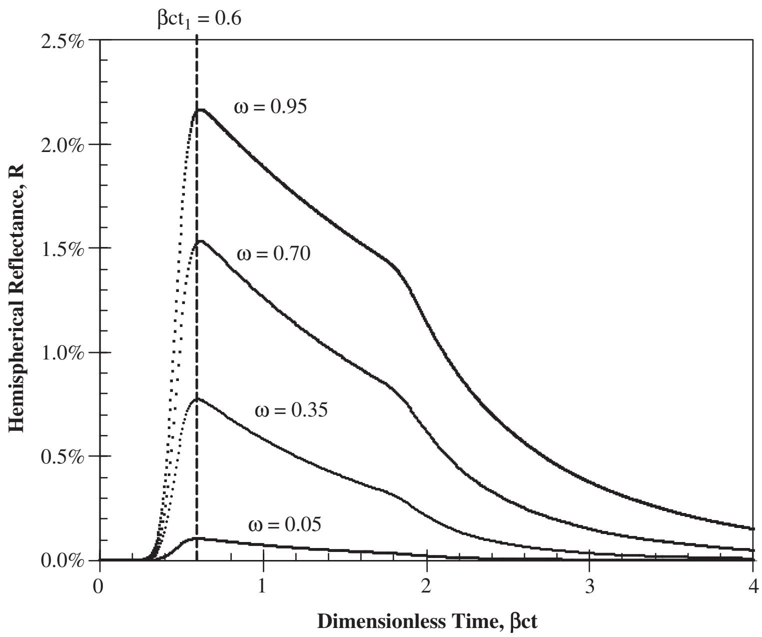


Fig. 3. Time-resolved hemispherical reflectance $R$ as a function of the dimensionless time $\beta ct$ for different values of $\omega$ and for $\beta L = 0.7$.

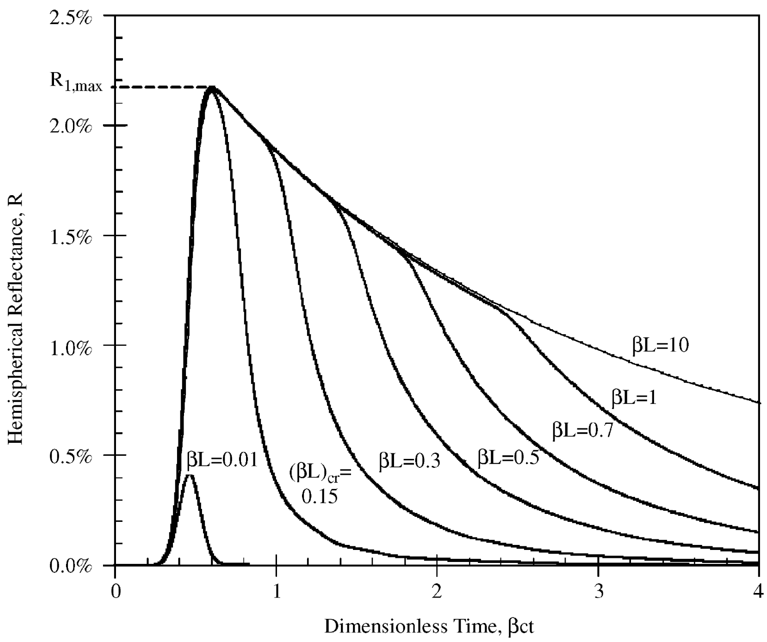


Fig. 4. Hemispherical reflectance $R$ as a function of $\beta ct$ for different values of $\beta L$ for $\omega = 0.95$ and $\beta ct_p = 0.15$.

the transient reflectance $R_1$ as a function of the optical thickness $\beta L$ ranging from 0.01 to 50 for $\beta ct_p = 0.15$ and for four different values of the single scattering albedo between 0.05 and 1. It also shows (bottom) the corresponding values of $\beta ct_1$ as a function of $\beta L$ for values up to 1 for the sake of clarity. The error bars correspond to a numerical uncertainty of $\pm 5\%$. It is interesting to note that the critical optical thickness $(\beta L)_{cr}$

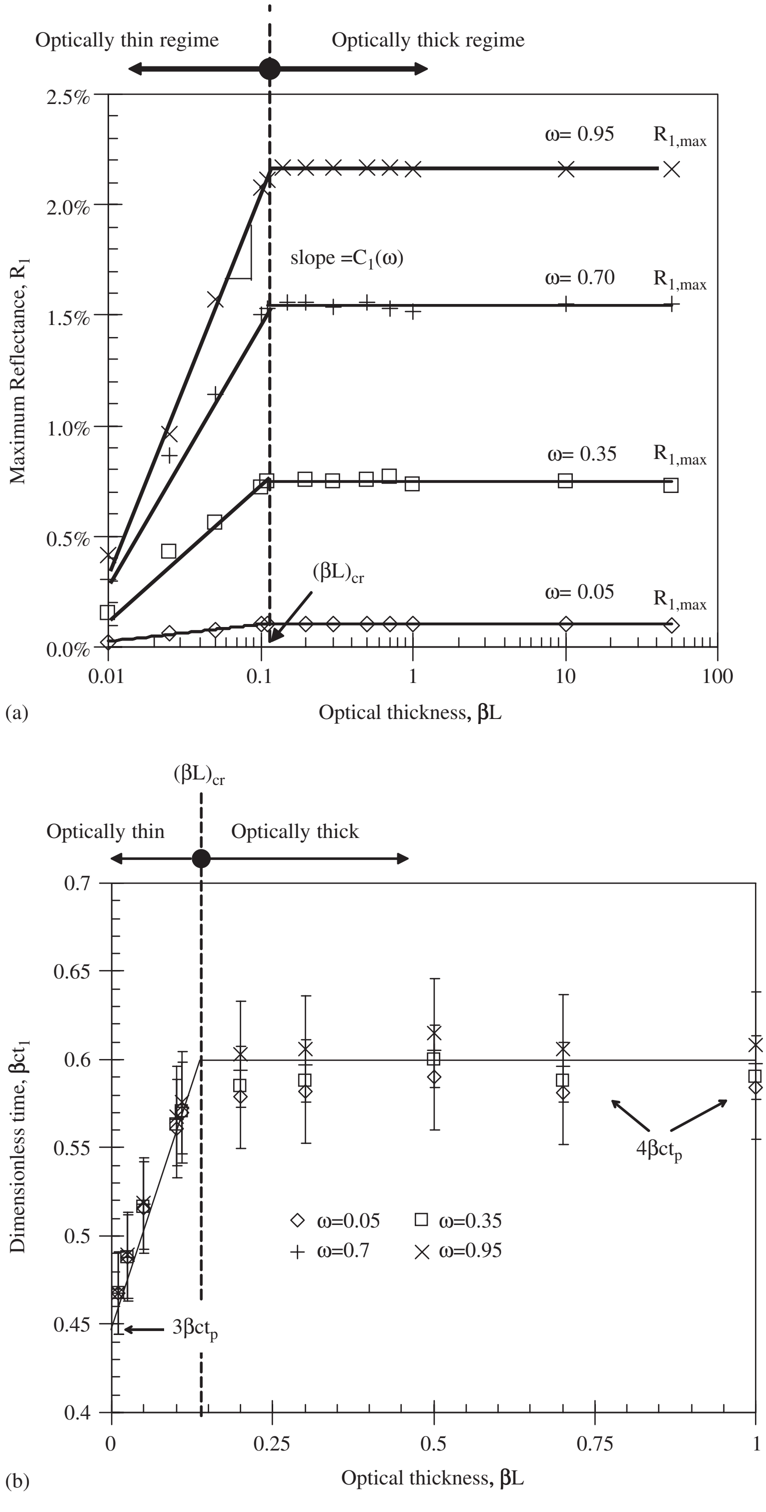


Fig. 5. Effect of the single scattering albedo $\omega$ and of the optical thickness $\beta L$ on the maximum reflectance $R_1$ (top) and the corresponding time $\beta ct_1$ (bottom) for $\beta ct_p = 0.15$.

is identical for $R_1$ and for $\beta ct_1$. Moreover, an optically thin and optically thick regimes can be identified as follows:

*Optically thin regime*: $\beta L \leqslant (\beta L)_{cr}$: In this regime, $R_1$ varies linearly with $\ln(\beta L)$ and increases as $\omega$ increases. On the other hand, $\beta ct_1$ is nearly independent of $\omega$ and varies linearly with $\beta L$. In addition, $(\beta L)_{cr}$ depends on the pulse width $\beta ct_p$.

*Optically thick regime*: $\beta L > (\beta L)_{cr}$: Beyond the critical value $(\beta L)_{cr}$, the optical thickness $\beta L$ has no effect on the maximum reflectance, and $R_1$ and $\beta ct_1$ reach their maximum denoted by $R_{1,max}$ and $\beta ct_{1,max}$, respectively. In this regime, $R_1$ is independent of $\beta L$ but increases with $\omega$. However, $\beta ct_1$ appears to be independent of both $\beta L$ and $\omega$.

### 4.3. Effect of the incident pulse width

To investigate the effect of the dimensionless pulse width on the hemispherical reflectance, different values of $\beta ct_p$ have been investigated, namely 0.15, 0.075, and 0.015. Fig. 6 plots $R_1$ versus $\beta L$ for different values of $\beta ct_p$ at $\omega = 0.7$. One can see that $R_1$ increases as $\beta ct_p$ increases for fixed values of $\omega$ and $\beta L$. This can be attributed to the fact that increasing the pulse width increases the radiant energy in the slab at any given time and, therefore, increases the scattered radiation intensity and the hemispherical reflectance.

In addition, Fig. 7 shows the ratio $\beta ct_1/\beta ct_p$ and $R_1$ as functions of $\beta L$ for different values of the single scattering albedo $\omega$. It indicates that as $\beta L$ tends to zero, $t_1$ tends asymptotically toward $3t_p$. Moreover, $\beta ct_1$ is independent of $\omega$ in the optically thin regime for all values of $\beta ct_p$. Additionally, once $\beta L$ reaches $\beta ct_p$, the value of $\beta ct_1$ and $R_1$ become independent of $\beta L$. This is defined as the optically thick regime because increasing $\beta L$ no longer has any effect on the values of $\beta ct_1$ and $R_1$. In the optically thick regime $\beta ct_1 = \beta ct_{1,max}$ and $R_1 = R_{1,max}$.

Finally, for each value of $\omega$, the values of $(\beta L)_{cr}$ can be obtained from $R_1$ versus $\beta L$ or from $\beta ct_1$ versus $\beta L$. The values of $(\beta L)_{cr}$ vary within 5% when obtained from either $R_1$ or $\beta ct_1$. Fig. 8 shows the average critical optical thickness $(\beta L)_{cr}$ as a function of the dimensionless pulse width $\beta ct_p$ for different values of $\omega$. One can

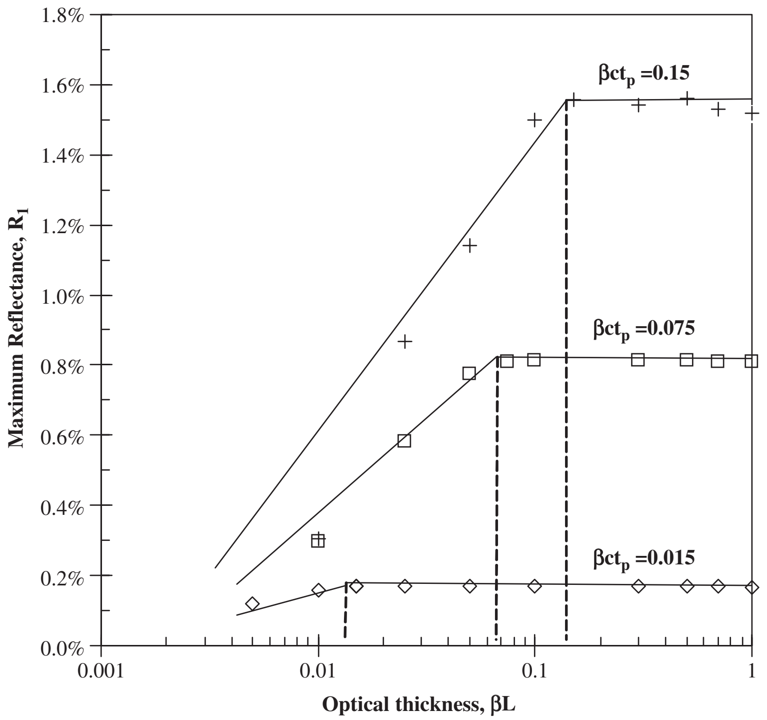


Fig. 6. Effect of the dimensionless pulse width $\beta ct_p$ on the maximum hemispherical reflectance $R_1$ for $\omega = 0.7$.

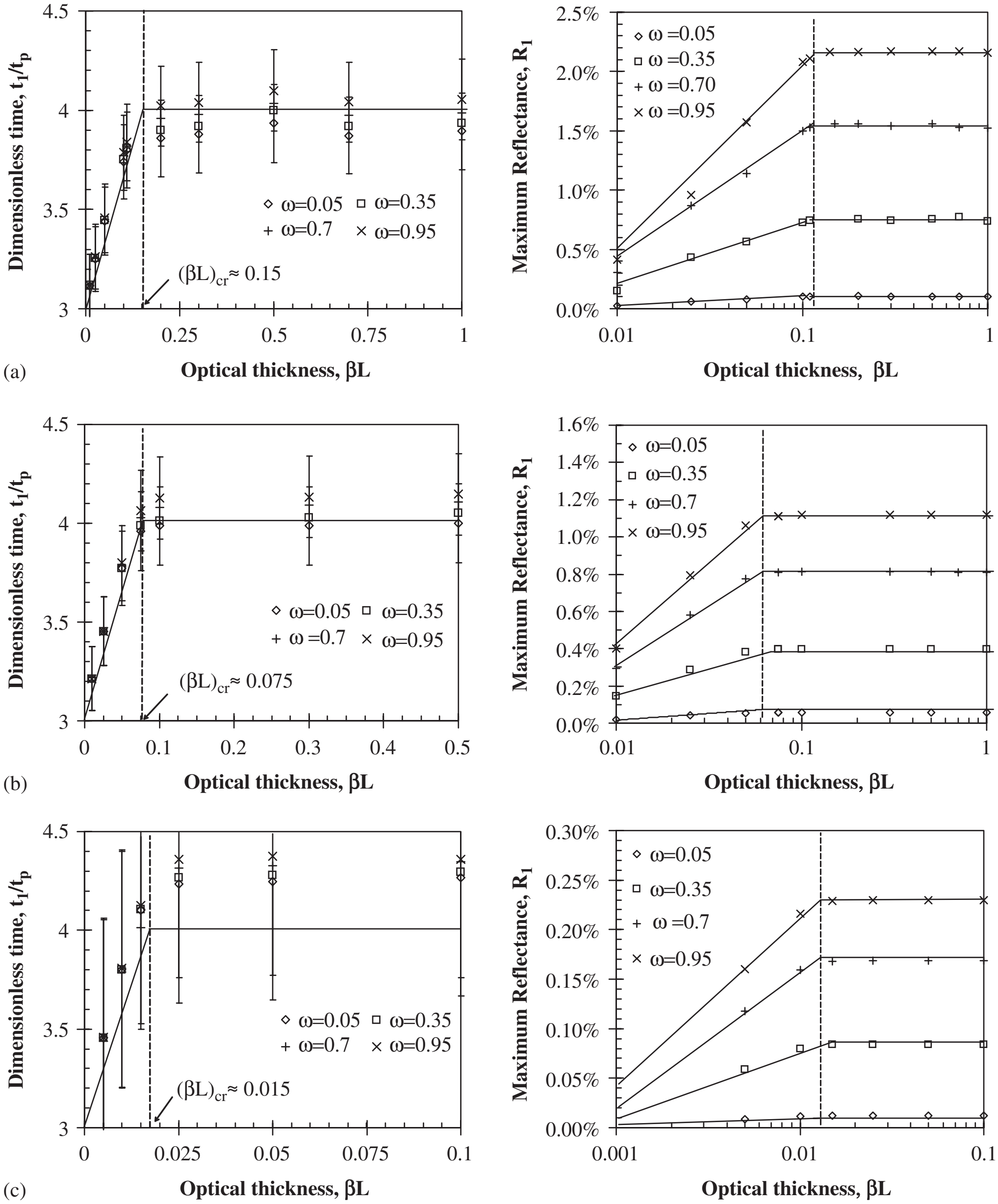


Fig. 7. $\beta ct_1/\beta ct_p$ and $R_1$ as functions of $\beta L$ and $\omega$ for (a) $\beta ct_p = 0.15$, (b) 0.075, and (c) 0.015. Error bars shown are the absolute errors.

see that for $\beta ct_p = 0.015$ and 0.075, the average value of the critical optical thickness $(\beta L)_{cr}$ is approximately $\beta ct_p$. However, when $\beta ct_p$ increases to 0.15, the average value of $(\beta L)_{cr}$ falls below $\beta ct_p$ possibly due to numerical error. Nonetheless, this finding indicates that $(\beta L)_{cr}$ is equal to $\beta ct_p$ within 10%.

### 4.4. Correlations

Developing correlations for transient hemispherical reflectance could be useful as a simple method for retrieving the optical thickness and the single scattering albedo of a substance. Then, each regime features its own set of correlations for $R_1$ and $\beta ct_1$.

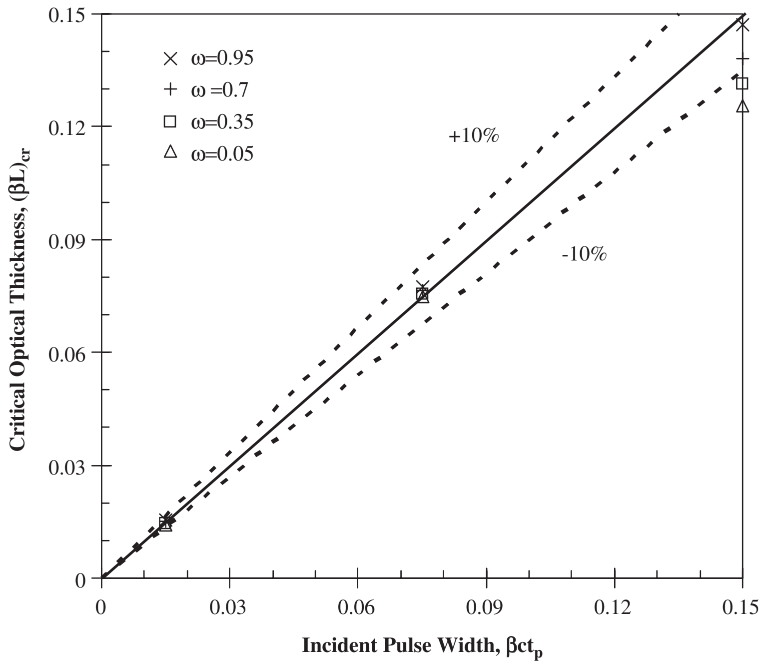


Fig. 8. Effect of the dimensionless pulse width $\beta ct_p$ and $\omega$ on the critical $\beta L$.

*Optically thin regime*: $\beta L \leqslant \beta ct_p$: In this regime the maximum reflectance $R_1$ varies as a function of $\ln(\beta L)$ as indicated by Figs. 5 and 6 and can be expressed as

$$R_1(\omega, \beta ct_p, \beta L) = C_1 \ln(\beta L) + C_2, \tag{6}$$

where the slope $C_1 = C_1(\omega, \beta ct_p)$ and the constant $C_2 = C_2(\omega, \beta ct_p)$ depend on both the single scattering albedo and the dimensionless pulse width. Fig. 9 illustrates $C_1/\beta ct_p$ and $C_2/\omega\beta ct_p$ as functions of $\omega$ and $\beta ct_p$, respectively, for $\beta L \leqslant \beta ct_p$. It shows that both $C_1$ and $C_2$ vary with $\omega\beta ct_p$ according to

$$C_1 = 0.05\omega\beta ct_p = 0.05\sigma_s ct_p, \tag{7}$$

$$C_2 = (-0.8\beta ct_p + 0.375)\sigma_s ct_p. \tag{8}$$

This confirms the finding that if the slab is non-scattering ($\sigma_s = 0$) its reflectance vanishes. The coefficients of regression $R^2$ for $C_1$ and $C_2$ are 0.998 and 0.973, respectively.

Similarly, Fig. 7 indicates that, within the numerical uncertainty,

$$\beta ct_1 = 3\beta ct_p + \beta L \quad \text{for } \beta L < \beta ct_p. \tag{9}$$

The value of $\beta ct_1 = 3\beta ct_p$ for the limiting case when $\beta L$ approaches 0 can be explained from first principles. Indeed, the scattered intensity in direction $\hat{\mathbf{s}}$ from a ray of radiation propagating in direction $\hat{\mathbf{s}}_i$ by an infinitesimally thin element dL can be expressed as [2]

$$\mathrm{dI_{sca}}(\hat{\mathbf{s}}, t) = \frac{\sigma_s \, \mathrm{d}L}{4\pi} \int_{4\pi} I(\hat{\mathbf{s}}_i, t)\Phi(\hat{\mathbf{s}}_i, \hat{\mathbf{s}}) \, \mathrm{d}\Omega_i, \tag{10}$$

when $\beta L$ approaches 0, one can safely assume that single scattering prevails [28]. Then, the incoming intensity from direction $\hat{\mathbf{s}}_i$ is identical to the incident intensity, i.e., $I(\hat{\mathbf{s}}_i, t) = I_i(t)\delta(\hat{\mathbf{s}} - \hat{\mathbf{s}}_0)$ and Eq. (10) reduces to, $I(\hat{\mathbf{s}}, t) = (\sigma_s L/4\pi)I_i(t)\Phi(\hat{\mathbf{s}}_0, \hat{\mathbf{s}})$. Then, using Eq. (5) for an isotropically scattering slab, the hemispherical reflectance simplifies to

$$R(t) = \frac{\sigma_s L}{2} \frac{I_i(t)}{I_0}. \tag{11}$$

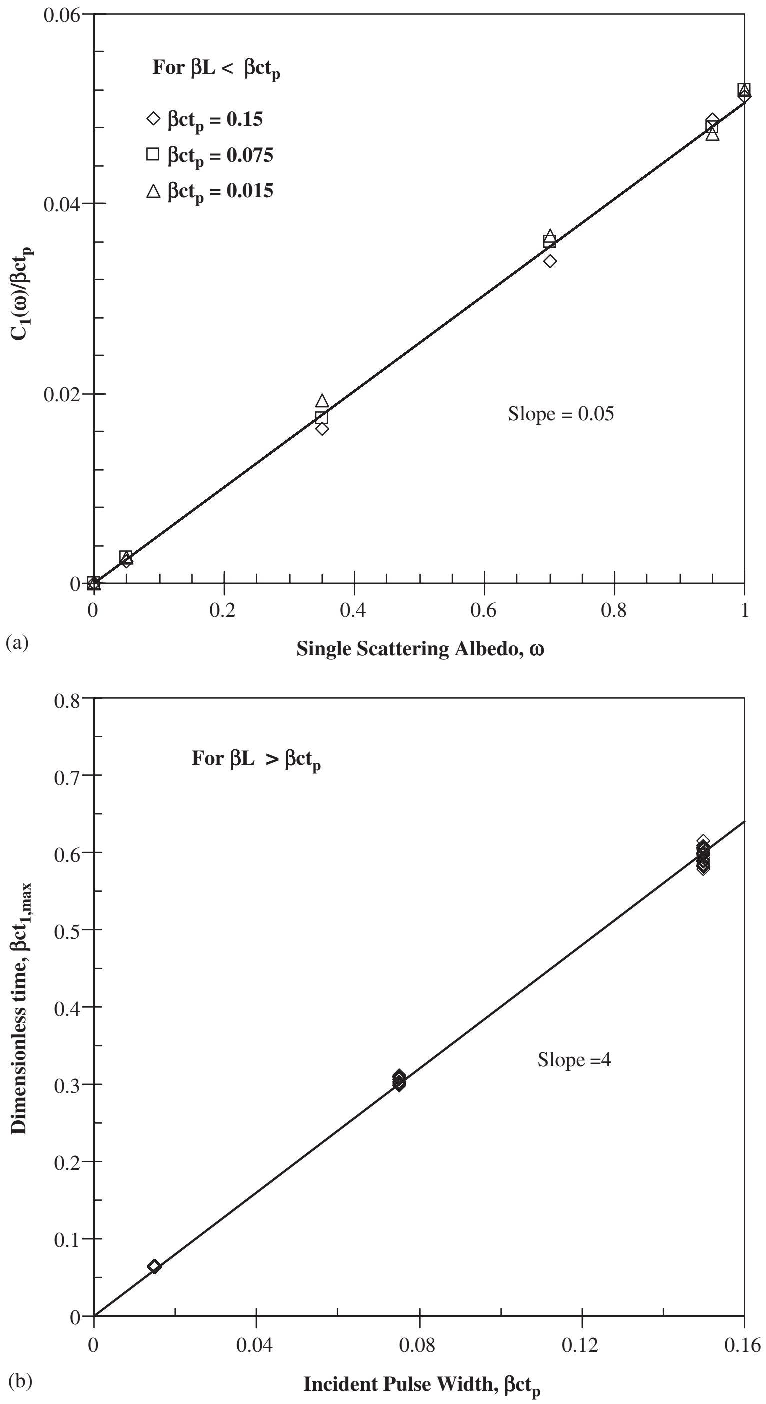


Fig. 9. Value of the slope $C_1/\beta ct_p$ and constant $C_2/\sigma_s ct_p$ as a function of the single scattering albedo, $\omega$, and the incident pulse width, $\beta ct_p$, respectively for $\beta L < \beta ct_p$.

Thus, the reflectance $R(t)$ is maximum when $I_i(t)$ is maximum, that is, when $t = t_c = 3t_p$, in our case. Moreover, predictions from Eq. (11) compare well with numerical results for $\beta L = 0.0001$ and $\beta ct_p = 0.015$. The maximum reflectance was $R_1 = 0.005\%$ and occurred at $\beta ct_1 = 0.0452$, with a relative error of 5.5% with respect to the predictions of Eq. (11).

*Optically thick regime*: $\beta L > \beta c t_p$: In this regime, the maximum reflectances $R_{1,\max}$ and $\beta c t_{1,\max}$ are independent of $\beta L$. Fig. 10 shows the linear increase of the ratio $R_{1,\max}/\beta c t_p$ as a function of $\omega$. It also shows $\beta c t_{1,\max}$ as a function of $\beta c t_p$ for all values of $\beta L$ and $\omega$ in this regime. It establishes that

$$R_{1,\max} = 0.156\sigma_s c t_p \quad \text{for } \beta L > \beta c t_p, \tag{12}$$

$$\beta c t_{1,\max} = 4\beta c t_p \quad \text{for } \beta L > \beta c t_p. \tag{13}$$

### 4.5. Discussion

First, numerical simulations were performed for different indices of refraction ($n = 1$, 1.33, and 1.5) for $\omega = 0.7$ and $\beta L = 0.5$ while still neglecting internal reflectance. This practically can be achieved by immersing the device in an index matching fluid whose index of refraction is the same as that of the slab to be analyzed. As expected from dimensional analysis, the same values of the transient hemispherical reflectance shown in Fig. 3 were obtained for the same set of parameters $(\omega, \beta L, \beta c t_p)$.

Moreover, Fig. 11 compares the predictions of the above correlations with numerically computed values of $R_1$ and $\beta c t_1$, respectively. The computed maximum hemispherical reflectance is properly predicted within a maximum absolute error of $\pm 0.21\%$, and every numerically computed dimensionless time $\beta c t_1$ is predicted within a maximum absolute error of $\pm 0.025$. The maximum relative error was determined for small values of $R_1$ that might be difficult to measure experimentally.

Additionally, the above correlations were validated against numerical results reported by Wu [9]. In particular Figures 3, 9, and 10 in Ref. [9] were digitized and the maximum reflectance was retrieved using digiXY. The optical thickness $\beta L$ ranged from 0.25 to 16, the single scattering albedo $\omega$ ranged from 0.05 to 1, and the dimensionless pulse width was either 0.15 or 0.3333 [29] while $t_c/t_p = 3$. Most data fell in the optically thick regime. The single scattering albedo was retrieved within 5% of its input value by recognizing that $\omega = 4R_{1,\max}/0.156\beta c t_{1,\max}$. If one assumes that $t_c$, $t_p$, $t_{1,\max}$, and $R_{1,\max}$ are accessible experimentally, the scattering coefficient $\sigma_s$ can be found from Eq. (12) within 16% of its input value. Moreover, we verified that $t_{1,\max} = t_p/4$ within 11%.

Finally, the above correlations could be used to determine the radiation characteristics of homogeneous absorbing and isotropically scattering media by experimentally measuring the maximum of the transient reflectance for slabs having at least two different thicknesses or by holding $t_c = 3t_p$ and varying the pulse width of the incident radiation. The slab thickness or the pulse width must be chosen in such a way to cover both the optically thin and thick regimes. Note that this bears some analogy with the method proposed by Yamada and Kurosaki [3] to retrieve the radiation characteristics of porous materials from *steady-state* emittance measurements. Indeed, the authors assumed an isotropic scattering phase function and used the fact that the emittance of an optically thick and isotropically scattering medium is independent of the optical thickness and depends only on the single scattering albedo. Alternatively, the method could also serve to obtain an initial guess for more complex inversion schemes accounting for anisotropic scattering.

## 5. Conclusions

This paper proposes a method to determine the radiation characteristics of homogeneous, cold, absorbing, and isotropically scattering plane-parallel slab with a transparent front surface and a black back surface from measured time-resolved hemispherical reflectance. It presents a parametric study focusing on the maximum hemispherical reflectance $R_1$ and its occurrence time $\beta c t_1$. Dimensionless parameters include the optical thickness of the slab $\beta L$, the single scattering albedo $\omega$, and the incident pulse width $\beta c t_p$. Conclusions of the study are as follows: (1) there exist optically thin and optically thick regimes for the maximum hemispherical reflectance $R_1$ and the dimensionless time $\beta c t_1$, (2) these two regimes meet at a critical optical thickness $(\beta L)_{cr}$ such that $(\beta L)_{cr} \approx \beta c t_p$, (3) in the optically thin regime, $R_1$ increases with increasing $\beta L$, $\omega$, and $\beta c t_p$, while $\beta c t_1$ is independent of $\omega$ but increases with $\beta L$ such that $\beta c t_1 = 3\beta c t_p + \beta L$, (4) in the optically thick regime, $R_{1,\max}$ is proportional to $\omega \beta c t_p$ and is independent of $\beta L$. On the other hand, $\beta c t_{1,\max}$ is independent of both $\omega$ and $\beta L$ such that $\beta c t_1 = 4\beta c t_p$.

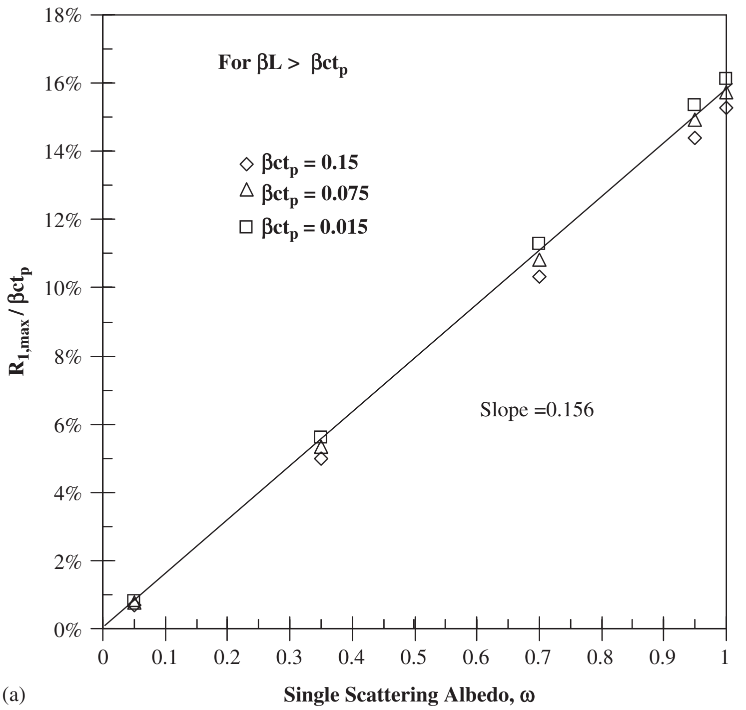


(a)

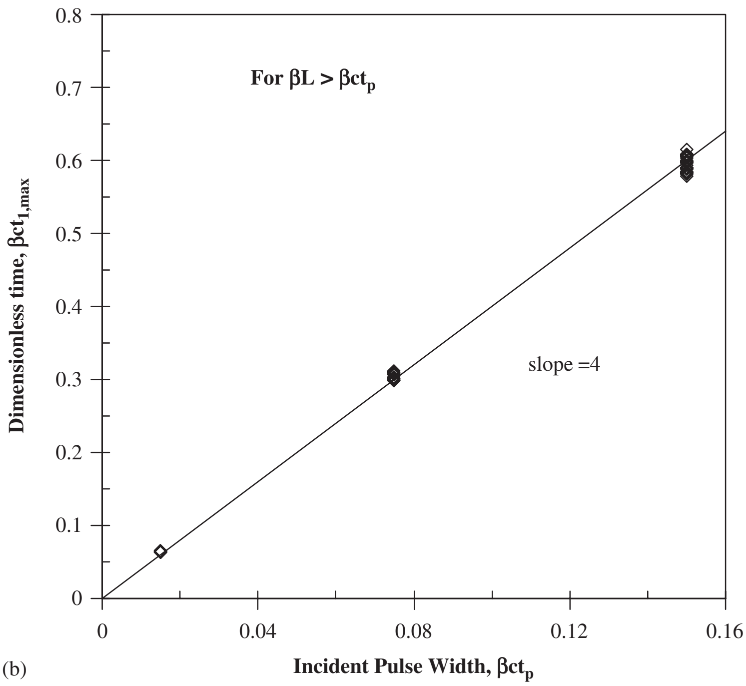


(b)

Fig. 10. Maximum hemispherical reflectance and $\beta ct_{1,\max}$ scaled with $\beta ct_{\rm p}$, as a function of the single scattering albedo $\omega$ in the optically thick regime ($\beta L > \beta ct_{\rm p}$).

Similar parametric studies could be performed for (i) other pulse shapes, (ii) independently varying $t_{\rm c}$ and $t_{\rm p}$ of the Gaussian pulse, (iii) cases when the indices of refraction across the front surface differ and one needs to account for internal reflection, and (iv) anisotropically scattering media. Similar trends and correlations are anticipated.

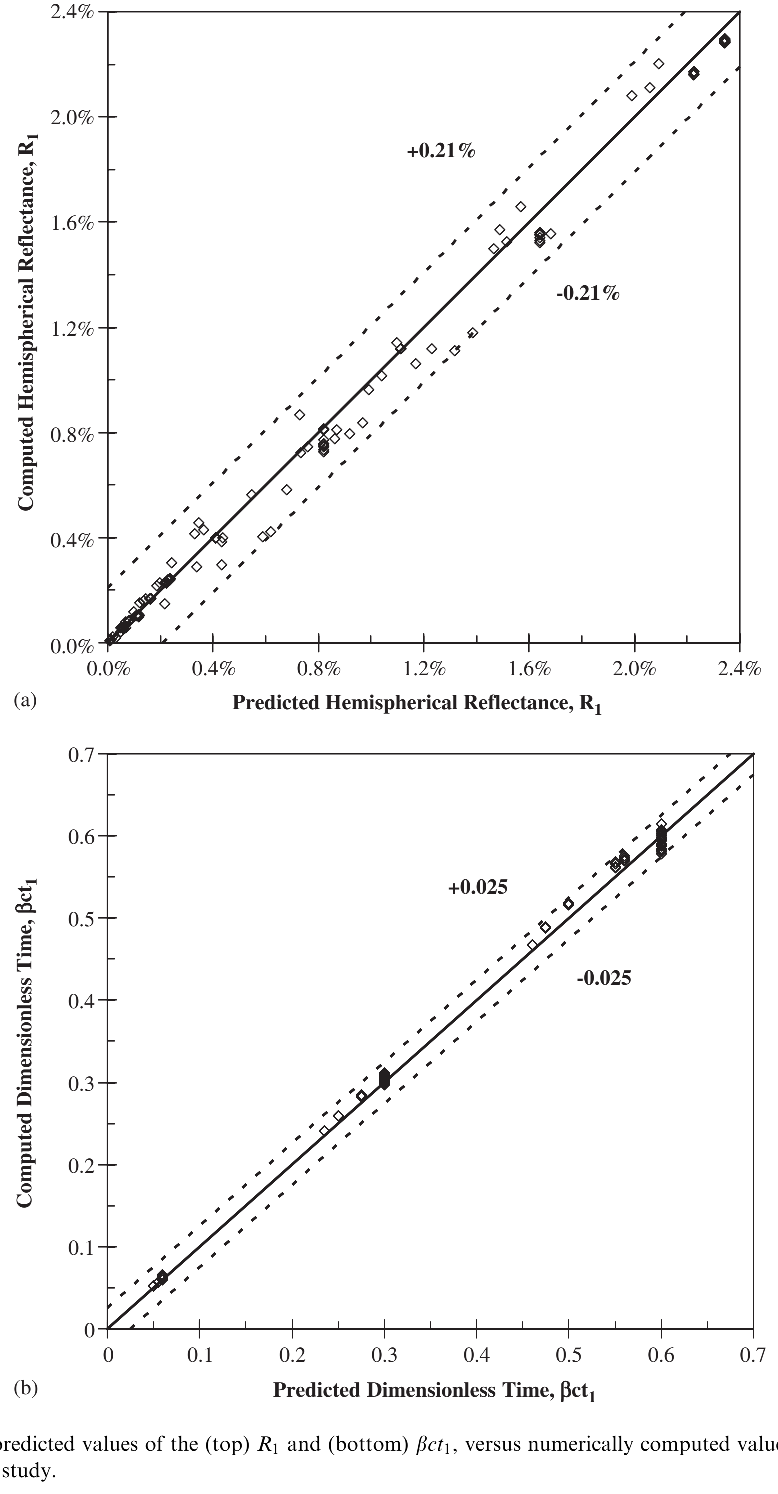


Fig. 11. Comparison of predicted values of the (top) $R_1$ and (bottom) $\beta ct_1$, versus numerically computed values for all values of $\beta L$, $\omega$, and $\beta ct_p$ explored in this study.

## References


[1] Kumar S, Mitra K. Microscale aspects of thermal radiation transport and laser applications. Adv Heat Transfer 1999;33:187–294.

[2] Modest MF. Radiative heat transfer. San Diego, CA: Academic Press; 2003.

[3] Yamada J, Kurosaki Y. Estimation of a radiative property of scattering and absorbing media. Int J Thermophys 1997;18(2):547–56.
[4] Patterson M, Chance B, Wilson B. Time resolved reflectance and transmittance for the non-invasive measurement of tissue optical properties. Appl Opt 1989;28(12):2331–6.
[5] Brewster MQ, Yamada Y. Optical properties of thick, turbid media from picosecond time-resolved light scattering measurements. Int J Heat Mass Transfer 1995;38:2569–81.
[6] Elaloufi R, Carminati R, Greffet JJ. Time-dependent transport through scattering media: from radiative transfer to diffusion. J Opt A: Pure Appl Opt 2002;4(5):S103–8.
[7] Guo Z, Kim K. Ultrafast-laser-radiation transfer in heterogeneous tissues with the discrete-ordinates method. Appl Opt 2003;42:2897–905.
[8] Pomraning GC. The equations of radiation hydrodynamics. New York, NY: Pergamon Press; 1973.
[9] Wu C-Y. Propagation of scattered radiation in a participating planar medium with pulse irradiation. JQSRT 2000;64(5):537–48.
[10] Tan Z-M, Hsu P-F. An integral formulation of transient radiative transfer. ASME J Heat Transfer 2001;123:466–75.
[11] Tan Z-M, Hsu P-F. Transient radiative transfer in three-dimensional homogeneous and non-homogeneous participating media. JQSRT 2002;73:181–94.
[12] Mitra K, Lai M, Kumar S. Transient radiation transport in participating media within a rectangular enclosure. J Thermophys Heat Transfer 1997;11:409–14.
[13] Guo Z, Kumar S, San K-C. Multidimensional Monte Carlo simulation of short-pulse transport in scattering media. J Thermophys Heat Transfer 2000;14(4):504–11.
[14] Guo Z, Kumar S. Three-dimensional discrete ordinates method in transient radiative transfer. J Thermophys Heat Transfer 2002;16(3):289–96.
[15] Hsu P-F. Effects of multiple scattering and reflective boundary. Int J Therm Sci 2001;40:539–49.
[16] Guo Z, Kumar S. Discrete-ordinates solution of short-pulsed laser transport in two-dimensional turbid media. Appl Opt 2001;40:3156–63.
[17] Guo Z, Kumar S. Three-dimensional discrete ordinates method in transient radiative transfer. J Thermophys Heat Transfer 2002;16:289–96.
[18] Guo Z, Kumar S. Radiation element method for transient hyperbolic radiative transfer in plane-parallel inhomogeneous media. Numer Heat Transfer: Part B 2001;39:371–87.
[19] Mitra K, Kumar S. Development and comparison of models for light pulse transport through scattering–absorbing media. Appl Opt 1999;38:188–96.
[20] Ayranci I, Selçuk N. MOL solution of DOM for transient radiative transfer in 3-D scattering media. JQSRT 2004;84:409–22.
[21] Chai JC, Hsu P-F, Lam Y. Three-dimensional transient radiative transfer modeling using the finite-volume method. JQSRT 2004;86:299–313.
[22] Boulanger J, Charette A. Reconstruction optical spectroscopy using transient radiative transfer equation and pulsed laser: a numerical study. JQSRT 2005;93:325–36.
[23] Lu X, Hsu P-F. Reverse Monte Carlo simulations of light pulse propagation within three-dimensional media. J Thermophys Heat Transfer 2005;19(3):353–9.
[24] Pilon L, Katika K. Backward method of characteristics for simulating microscale energy transport. ASME J Heat Transfer 2004;126:735–43.
[25] Katika K, Pilon L. Modified method of characteristics for transient radiative transfer. JQSRT 2006;98:220–37.
[26] Katika K, Pilon L. Backward method of characteristics in radiative heat transfer. In: Fourth international symposium on radiative transfer, Istanbul, Turkey, June 18–21, 2004. p. 347–55.
[27] Hoffman JD. Numerical methods for engineers and scientists. New York NY: McGraw-Hill; 1998.
[28] Tien CL, Drolen BL. Thermal radiation in particulate media with dependent and independent scattering, Annu Rev Numer Fluid Mech Heat Transfer 1987;1:1–32.
[29] Wu C-Y. Personal communication regarding Ref. [10], December 2003.